JAAS

PAPER

View Article Online
View Journal | View Issue

Cite this: J. Anal. At. Spectrom., 2024, 39, 962

A chemically functionalized glass support for gold and silver metallic nanoparticle analysis with LIBS

J. Cárdenas-Escudero, [ae] V. Gardette,[b] A. Villalonga,[c] A. Sánchez,[c] R. Villalonga, *[c] V. Motto-Ros, *[b] D. Galán-Madruga *[d] and J. O. Cáceres *[a]

This work has focused on the development of a new analytical alternative based on the laser-induced breakdown spectroscopy (LIBS) technique for the fast, reliable, and economical determination of the gold and silver nanoparticle content in a low linear concentration range between 2.9 and 0.058 μg mL^{-1} and 2.9–0.116 μg mL^{-1}, respectively, without requiring complicated sample pretreatment procedures or advanced separation techniques. Metallic nanoparticles are currently essential materials for the development of new technologies in different scientific and technical areas. However, numerous studies have pointed out these nanomaterials' toxic and polluting potential and the various health implications for humans, animals, and the ecosystem. The current reality reflects the lack of analytical techniques with low economic, environmental, and health impacts and the capacity to quantify the total metallic nanoparticle content. For this purpose, a novel and simple method for the selective capture of gold and silver nanoparticles, consisting of a chemically functionalized glass surface, has been custom-developed for subsequent analysis with LIBS. The results show that the proposed method, employing a functionalized sample glass support, presents a suitable analytical performance characterized by increased sensitivity, specifically 4.7% and 329.2% for Au-NPs and Ag-NPs, and proportionally decreased error in the slope and intercept of the calibration curves, 68% for Au-NPs and 87% for Ag-NPs, respectively.

Received 30th November 2023
Accepted 6th February 2024

DOI: 10.1039/d3ja00425b

rsc.li/jaas

1. Introduction

1.1. The emerging analytical issues and concerns around gold and silver nanoparticles

Metallic nanoparticles (NPs) are a specific type of nanomaterial, typically consisting of metal particles between 1 and 100 nanometres in size. Because of their small size, they have unique physical and chemical properties that differ from those of larger particles of the same material. These properties are largely due to the fact that the surface-to-volume ratio of nanoparticles is much higher than that of larger particles. Currently, researchers are focusing on metallic nanoparticles due to their appealing properties, which are useful for catalysis,[1–3] preparation of composites such as polymers,[4] disease diagnosis and treatment,[5–7] sensor technology, and labelling of optoelectronic substrates.[1,8]

Within the wide range of solid metallic nanoparticles available, gold nanoparticles are the most widely studied and used in the scientific field, given their unique optical, photothermal, and electronic properties.[9,10] In addition, solid gold nanoparticles have diversified so much over time that they are now widely used for novel applications ranging from drug delivery and therapy strategies to specialized sensors for imaging.[9] Silver nanoparticles are another typical example of solid metallic nanoparticles, which, unlike gold, owe their popularity to their bactericidal,[11,12] catalytic,[12] anti-inflammatory,[13,14] and other medical[13] properties. However, the widespread use of nanoparticles has led to some opinions and evidence about the potential of solid metallic nanoparticles as toxic agents[15–17] for human health[16–22] and as pollutants in the environment,[16,21,23] especially water.[21]

Despite the rapid dissemination of the use of nanoparticles of gold, silver, and other metals, the quantification of these nanomaterials is a major analytical challenge, mainly due to their characteristic size and the lack of highly sensitive detection systems that guarantee a high degree of precision and accuracy that this type of analysis requires. One of the main problems associated with the quantification of metal nanoparticles is the selection of separation and pre-concentration

[a]Laser Chemistry Research Group, Department of Analytical Chemistry, Faculty of Chemistry, Complutense University of Madrid, 28040, Madrid, Spain. E-mail: jcaceres@ucm.es

[b]Institut Lumière Matière UMR 5306, Université Lyon 1 – CNRS, Université de Lyon, Villeurbanne, France. E-mail: vincent.motto-ros@univ-lyon1.fr

[c]Nanosensors and Nanomachines Group, Department of Analytical Chemistry, Complutense University of Madrid, 28040, Madrid, Spain. E-mail: rvillalonga@quim.ucm.es

[d]National Centre for Environmental Health, Carlos III Health Institute, Ctra. Majadahonda-Pozuelo km 2.2, Majadahonda, 28220, Madrid, Spain. E-mail: DAVID.GALAN@isciii.es

[e]Analytical Chemistry Department, FCNET, Universidad de Panamá, Manuel E. Batista and José De Fábrega av., Ciudad Universitaria, Estafeta Universitaria, Bella Vista, 3366, Panamá 4, Panama

techniques for nanoparticles, although nowadays, there are several physical separation techniques, such as ultrafiltration, ultracentrifugation, and centrifugal ultrafiltration. Furthermore, other chemical separation techniques, such as hydrodynamic chromatography (HDC) and electrophoresis, can have better or worse performance depending on the characteristics of the NPs, such as their size, external coating, shape, *etc.*,[24] which is a major complication in the pre-analytical stage. In this sense, the development of new analytical mechanisms that allow the selective trapping of nanoparticles for their subsequent qualitative or quantitative determination is key for this type of analysis, which is so important in the scientific, clinical, and environmental fields. However, the LODs associated with the quantification of total Au-NP and Ag-NP content using these conventional separation techniques, such as liquid or solid phase extraction, are not as low as those obtained with newer extraction methods, such as point-cloud extraction (CPE)[25] or with the preferred field-flow fractionation (FFF) technique,[26] which are employed with ICP-MS-based detection. The total NP content is usually determined by using optical emission spectrometry techniques, such as inductively-coupled plasma mass spectrometry (ICP-MS) or surface plasmon resonance (SPR). In the specific case of ICP-MS, when used with other separation techniques, such as those mentioned above, it provides appropriate sensitivity for the quantification of metallic nanoparticles.[24] However, the detection limit of this technique is highly dependent on the efficiency and sophistication of the separation and sample pretreatment methods, and their use is a major limitation due to the requirement for highly specialized and expensive instrumentation, which prevents them from being an environmentally friendly and economically viable option, not to mention the significant time that can be consumed in the use of this advanced technique and their high cost. All this together makes the detection of metallic NPs by ICP-MS-based techniques a not very efficient option. On the other hand, a problem associated with the use of the SPR technique for the quantification of the total NP content is the presence of the plasmons of the NPs as a band in the UV-vis spectral range that allows the determination of the concentration.

Introducing the use of the laser-induced breakdown spectroscopy (LIBS) technique for the quantification of MNPs is an analytically strategic and viable option due to the almost null sample treatment[27] required for the analysis and the high sensitivity of the technique for the detection of metallic species,[28–31] based on the capture of the spectral information of the plasma that is generated on the surface of the sample when a pulsed laser is previously incident on it. Relevant studies that serve as a background for the use of LIBS for the quantification of NPs have focused on the use of MNPs on the surface of metallic samples for the study of the improvement of the analytical signal obtained due to the presence of nanoparticles, which has allowed the development of a variant of the LIBS technique known as nanoparticle enhanced laser induced breakdown spectroscopy, NELIBS.[32,33] In addition to presenting significant results related to the analytical suitability of the LIBS technique for the preliminary characterization of Ag-NPs, one of the most interesting inferences of these studies refers to the influence of NP size on the slope of the calibration curve for the characterization of NPs by LIBS, which has been an important limitation for the development of the LIBS technique as a viable alternative for the characterization of real samples, with unknown content and size of nanoparticles. These results suggest the need for analytical strategies conveniently designed to overcome this limitation that has made it impossible to use the LIBS technique to quantify the total NP content in real samples.

Thus, this work has focused on the development of a fast, reliable, and economically easy-to-perform analytical application based on LIBS for the analysis of gold and silver nanoparticles by employing, for the first time, a chemically functionalized glass support that enables selective trapping and fixation of NPs to the glass sample support surface, without the need for complex sample pretreatment or the use of advanced separation techniques.

2. Materials and methods

2.1. Synthesis of citrate-capped Au-NPs

Citrate-capped Au-NPs were prepared according to previous studies.[34] First, 100 mL of an aqueous solution of $HAuCl_4$ (0.01%) (Alfa Aesar) was heated to boiling, and then 5 mL of an aqueous solution of trisodium citrate (1%) (Sigma-Aldrich) was added. After 10 minutes of boiling, the mixture was cooled to room temperature. The Au-NP nominal concentration in the final solution was 58.0 $\mu g\ mL^{-1}$.

2.2. Synthesis of citrate-capped Ag-NPs

Citrate-capped Au-NPs were prepared according to Mendi's approach.[35] 5 mL of an aqueous solution of silver nitrate (0.017%) (Alfa Aesar) was dropped into 50 mL of a stirred aqueous solution of trisodium citrate (0.155%) and $NaBH_4$ (0.0045%) (Scharlau). After 30 min of stirring, citrate-capped Au-NPs were collected by centrifugation, washed with trisodium citrate (0.26%), and finally suspended in 2 mL of trisodium citrate (0.775%). The Ag-NP nominal concentration in the final solution was 0.27 $mg\ mL^{-1}$.

2.3. NP characterization method

The concentration of the prepared NP solutions was determined by the UV-vis spectroscopy method, based on the extinction coefficient determination for gold[36] and silver[37] nanoparticles, with an Ultrospec 8000 spectrometer (GE Healthcare Life Sciences, Buckinghamshire, UK), equipped with a double-beam monochromator, a deuterium + tungsten light source, and a dual-silicon-photodiode-based detector. The spectra were collected with ± 0.3 nm wavelength accuracy across the wavelength range, with ± 0.1 nm wavelength reproducibility, and ± 0.002 photometric reproducibility.

Regarding the particle size, the prepared NP stock solutions were characterized by the ultra-high resolution transmission electron microscopy technique (TEM) using an analytical transmission electron microscope JEM 2100 (JEOL, Ltd, Tokyo,

Japan) equipped with a LaB_6 thermionic electron gun, an accelerating voltage of 200 kV, a built-in scanning-transmission electron microscopy (STEM) unit with a brightfield detector with 0.25 nm between spots, and an X-ray energy dispersive spectroscopy microanalysis system (XEDS-OXFORD INCA). The images were collected using the built-in CCD ORIUS SC1000 (Model 832) camera. The samples were prepared by depositing gold and silver nanoparticle stock solution drops, separately, on a copper grid covered with a carbon film.

2.4. Chemical functionalization of the glass support

Microscope glass slides were chemically functionalized according to Marques's method by silane coupling reactions.[38] The glass surface was activated by immersion in an aqueous solution of nitric acid (20%) (Scharlab) at room temperature for 24 hours. After this, the slides were extensively washed with type 1 water (Merck Milli-Q IQ 7000 model ultrapure water system, Darmstadt, Germany). Then, the slides were immersed in an H_2O_2 aqueous solution (10%) (Sigma-Aldrich) at 75 °C. After 45 minutes, the slides were cooled at room temperature, and 5 mL of concentrated NH_4OH solution (Scharlau) was added. Then, the slides were widely washed with type 1 water and finally with methanol (Sharlau). To graft the silane (–SiO_3 groups), a solution of 25% methanol in water, with a previously adjusted pH of 4.5 using acetic acid, was used to dissolve 3-(mercaptopropyl) trimethoxysilane (Alfa Aesar) to reach a final concentration of 2%. After stirring this solution for 10 min, the glass slides were immersed in the 2% silane solution for 30 min, and then rinsed with ethanol (96%, Scharlau) and aged at 110 °C for 30 min. Additionally, atomic force microscopy images were obtained to confirm the attachment and distribution of the NPs on the surface of the functionalized glass support before and after depositing the nanoparticle solution in the support. For this purpose, an atomic force microscope AFM multimode Nanoscope III A (Bruker, Massachusetts, USA) was used with three scanners of 1 μ, 15 μ, and 150 μ with contact and tapping modes with nanometric resolution.

2.5. Nanoparticle sample preparation and analysis procedure

Ten working solutions of known concentration were prepared from the gold and silver nanoparticle solutions, specifically 2.900, 1.740, 0.580, 0.116, and 0.058 μg mL^{-1} for gold nanoparticles, and 2.900, 1.740, 1.160, 0.580 and 0.116 μg mL^{-1} for silver nanoparticles. Then, with the help of double-sided adhesive tape, wells of 4 mm were delimited to deposit 4 μL drops in triplicate for each nanoparticle working solution on the surface of the glass previously functionalized with the silane group. In this way, droplet runoff was avoided, and the concentration of the nanoparticles in the well area was enhanced. Fig. 1 shows the schematic of the sample preparation.

Once the drops of the working solutions for gold and silver nanoparticles were deposited, they were allowed to dry at room temperature in a clean, contamination-free area. Once the droplets were completely dried on the functionalized glass support, they were analyzed with the μLIBS imaging technique. This experiment was carried out on functionalized and non-functionalized glass supports. The glass support was placed on the LIBS instrument platform, and the entire surface of the glass was ablated, except for the frosted area where no nanoparticles were deposited. For each well, 31 000 spectra were obtained, in addition to the spectra of the area of the glass support surface where no signal was detected for the analytes of interest.

2.6. μLIBS-imaging instrumentation and technical parameters

The μLIBS-imaging instrument consisted of a multimode 1064 nm IR laser source with a pulse duration of 8 ns, a maximum pulse energy of 2 mJ, and a repetition frequency of 100 Hz. The analysis sequence was adjusted to a pulse resolution of 35 μm, and all measurements were performed at room temperature and assisted with a 0.8 L mm^{-1} flow of ultra-high purity compressed argon gas. The detection system consisted of a Shamrok 500 spectrometer with an intensified charge-coupled device (ICCD), with a delay and gate acquisition setting of 1 μs and 5 μs, respectively, and a grating adjusted to 2400 L mm^{-1}. This configuration results in 31 000 spectra per well, each at different locations of the glass surface to avoid depletion or crater formation in the sample surface. The spectral window selected was 257.60 nm–277.50 nm and 327.07 nm–336.50 nm for Au-NPs and Ag-NPs, respectively, according to the NIST LIBS database[39] for the Au and Ag emissions lines.

2.7. Data treatment and analysis

The acquisition and data analysis were performed using a custom-developed LabVIEW software (National Instrument, Ireland). During the μLIBS-imaging analysis, the following approach was used to process the spectra. Initially, all spectra obtained were subjected to a baseline adjustment pretreatment. Next, the spectra corresponding to each droplet were averaged ($n = 31\,000$). Then, the mean spectra for each triplicated drop were averaged ($n = 3$) for the five concentration levels used in the working solutions for gold and silver nanoparticles. The average spectrum quantitative data for each concentration level were determined by using the average intensity ($n = 3$) of the emission lines corresponding to gold and silver, *i.e.*, 267.59 nm and 328.15 nm, respectively, according to the NIST LIBS database.[39] The calibration curves were constructed with this intensity information as a function of gold and silver concentration.

3. Results and discussion

3.1. Au-NP and Ag-NP characterization and their interaction with the functionalized glass support

The NPs prepared for this research were characterized using the procedure described in Section 2.3. The average metallic concentration results obtained with the UV-vis spectroscopic method for Au-NPs[36] and Ag-NPs[37] were 58 ± 3 μg mL^{-1} and 27 ± 2 mg mL^{-1}, respectively. The UV-vis spectra of the

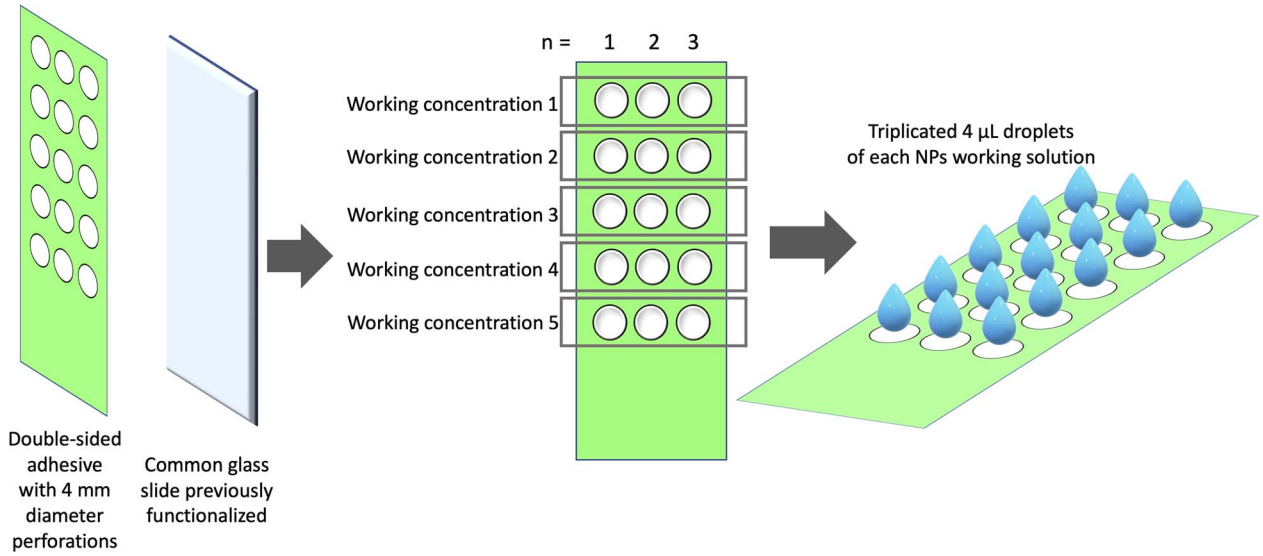

Fig. 1 A schematic of the custom-designed silane-functionalized glass support and sample preparation procedure was developed in this research for the LIBS-based nanoparticle analysis.

nanoparticles are shown in Fig. 2. For the gold nanoparticle suspension, it is observed that the maximum absorbance at 520 nm is congruent with the particle size observed in the subsequent TEM analysis results (Fig. 3). According to the bibliography, gold nanoparticle solutions with diameters between 12 and 41 nm show an absorption maximum between 520 and 530 nm.[40] On the other hand, the UV-vis spectrum of the prepared silver nanoparticle suspension shows a maximum at 391 nm, consistent with the particle size observed in the subsequent TEM images (Fig. 3). These results are also in line with previous studies that have experimentally established that a silver nanoparticle suspension with an absorption maximum at 390 nm is due to particle sizes averaging around 20 nm.[41]

The size characterization results of the prepared nanoparticles, presented in Fig. 3, were obtained with the procedure described in Section 2.3. These results show the high sphericity and homogeneity among the prepared nanoparticles, with an average particle size of 19 ± 1 nm and 23 ± 2 nm for Au-NPs and Ag-NPs, respectively.

These promising results concerning the low size dispersion in the prepared NPs and their significant spherical homogeneity are the result of the use of NP preparation methods that have been extensively studied and whose effectiveness has been validated in several previous studies: the Turkevich[42–46] and Mendi's[35,47] methods for Au-NP and Ag-NP preparation, respectively.

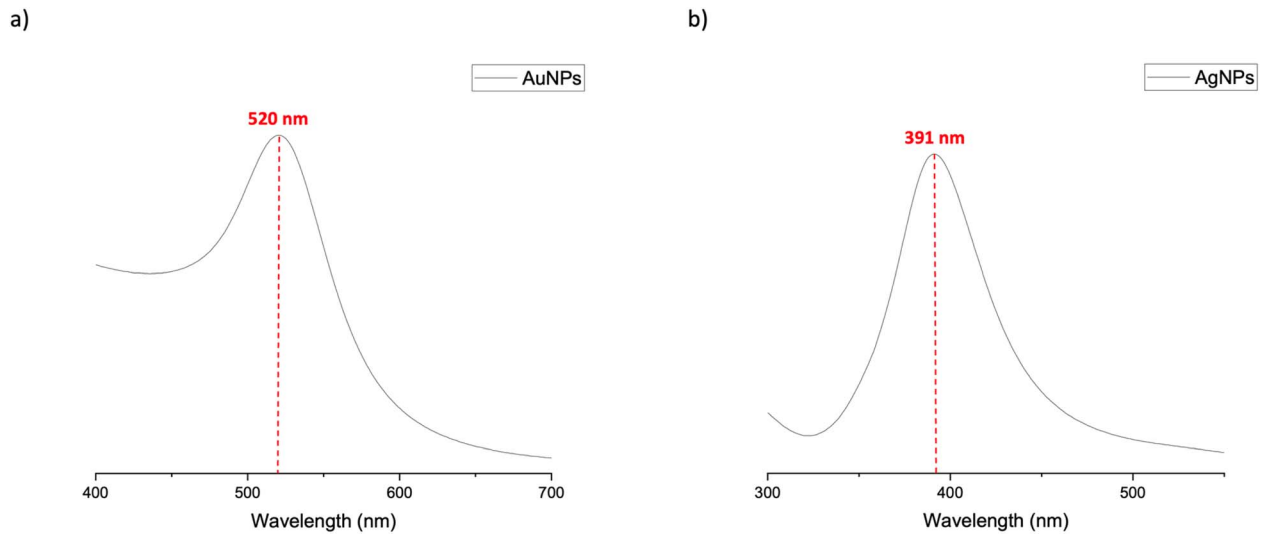

Fig. 2 NP concentration determination by the UV-visible method for gold[36] and silver[37] nanoparticles: (a) Au-NP stock solution spectrum. (b) Ag-NP stock solution spectrum. The average concentration results obtained with the UV-vis spectroscopic method for Au-NPs[36] and Ag-NPs[37] were 58 ± 3 µg mL^{-1} and 27 ± 2 mg mL^{-1}, respectively.

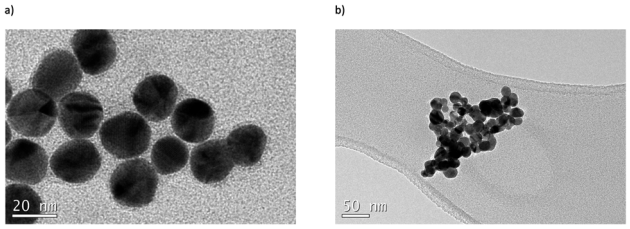

Fig. 3 NP characterization using the analytical transmission electron microscopy (TEM) technique. (a) UHR-TEM image of the prepared Au-NPs and (b) TEM image of the prepared Ag-NPs used in this research. The results showed an average particle size of 19 ± 1 nm and 23 ± 2 nm for Au-NPs and Ag-NPs, respectively.

On the other hand, about the study of the interaction of the prepared nanoparticles with the functionalized glass surface, Fig. 4 shows the atomic force microscopy (AFM) images of the silane-functionalized glass support, custom-designed for the LIBS-based metallic nanoparticle analysis, with and without Au-NP and Ag-NP colloidal solution deposition. These results evidence the attachment of the nanoparticles to the glass support, regardless of size, enabled by prior functionalization with silane groups.

This is perhaps one of the most important results of the study since it is the first time that this type of functionalized sample support has been applied for the analysis of nanoparticles by LIBS. This simple yet analytically strategic mechanism for nanoparticle attachment based on surface functionalization is widely employed for constructing optical and electrochemical-based biosensors and sensors today,[48–51] among other relevant applications.[52–54] In the case of this study, thiol groups chemically bonded to the glass support have been used to enable the selective capture of gold and silver nanoparticles on the surface support, as shown in Fig. 5, by interaction with the terminal sulfhydryl (–SH) functional groups in thiol (R-SH) groups on the surface of the designed support.[55–57]

Incorporating functionalities on the glass surface, composed of silica, is possible using different routes.[57] However, the traditional techniques of silica surface modification involve the use of the grafting method (Fig. 5), widely used for the immobilization of metallic nanoparticles for the development of sensors and biosensors, employing compounds such as silazanes, chlorosilanes, or organosilanes,[57] as the thiol-terminated 3-(mercaptopropyl) trimethoxysilane coupling agent used in this study.

This silane grafting enables the chemical reaction of free terminal sulfhydryl (–SH) functional groups in the grafting molecule (3-(mercaptopropyl) trimethoxysilane) used for the functionalization of the surface of the designed support[55–57] (Fig. 5d) which in turn functions as a "chemical adhesive" for the Au-NPs or Ag-NPs on the functionalized glass surface, as presented in Fig. 5e, due to the high chemical affinity between sulfur and gold[58,59] and silver[60,61] nanoparticles, which results in strong and stable Au–S[59] and Ag–S bonds[62] indistinctly regardless of their NP size. More detailed information about the surface functionalization strategy used in this work can be found in ref. 57, 63 and 64.

Since the surface grafting procedure performed as part of the glass surface functionalization allows a homogeneous distribution of the terminal –SH functional groups on the surface of the material (Fig. 5c), the distribution of the entrapped nanoparticles is also mainly homogeneous[55] (Fig. 5e), as shown in

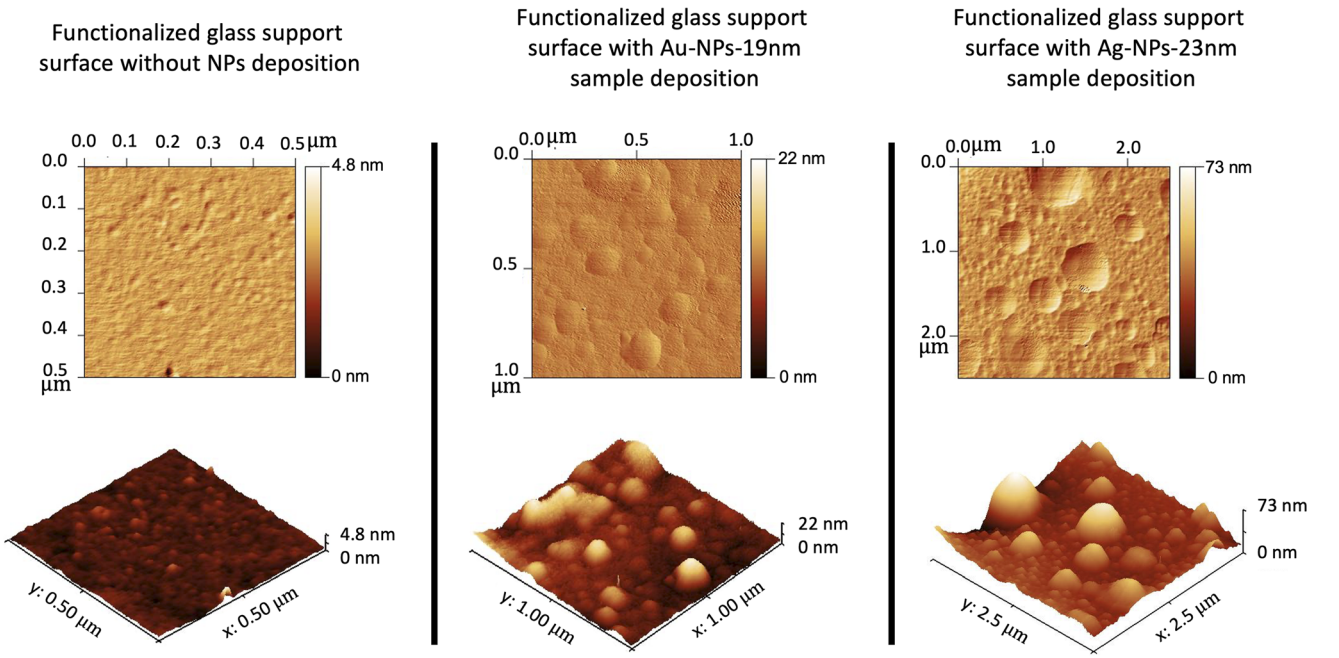

Fig. 4 Representative atomic force microscopy (AFM) images of the silane-functionalized glass support, custom-designed in this research for the LIBS-based metallic nanoparticle analysis. The left part shows the functionalized surface without nanoparticles. The middle part shows the surface once the Au-NPs have been deposited. Finally, the functionalized surface with the deposited Ag-NPs is observed in the right part.

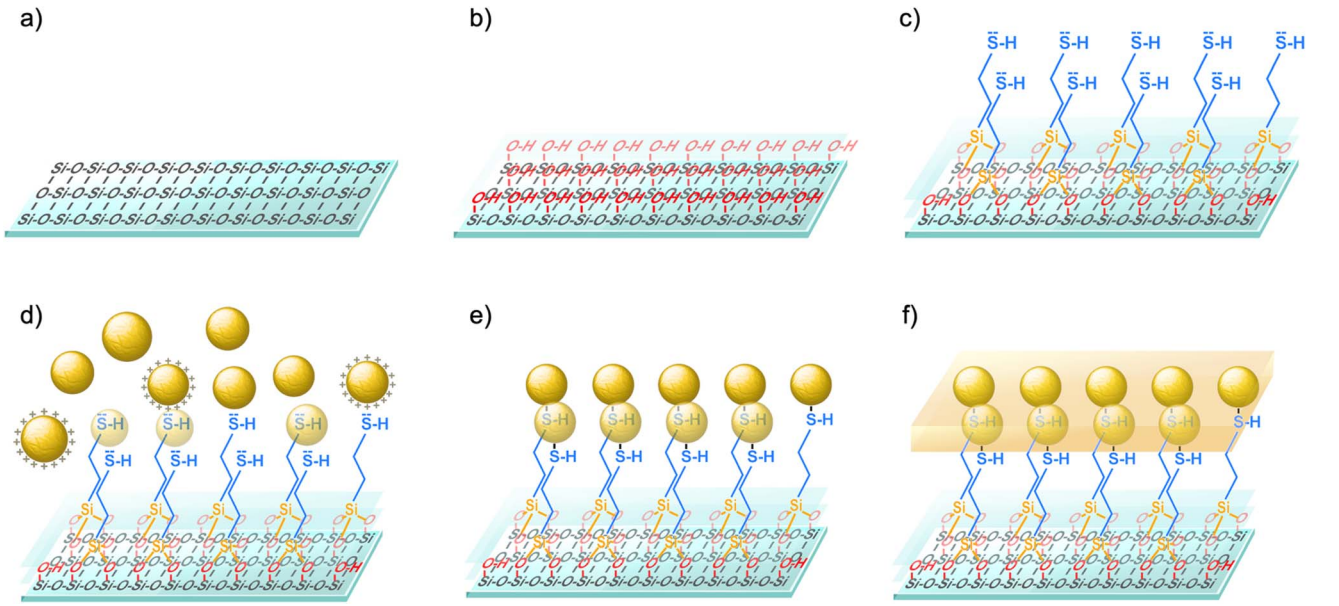

Fig. 5 Graphical representation of the glass surface functionalization process and the selective trapping mechanism of metal nanoparticles detailed in Section 2.4. (a) Glass surface support activation by immersion in an aqueous nitric acid solution. (b) Hydroxylation of the activated glass surface by treatment with H_2O_2 and NH_4OH. (c) Glass surface silanization by treatment with 3-(mercaptopropyl) trimethoxysilane. (d) Electrostatic interaction of terminal sulfhydryl (–SH) groups with the surrounding metal nanoparticles. (e) Metallic nanoparticle assembly on the functionalized glass surface by Au–S bond formation. (f) Metallic nanoparticle self-assembled monolayer formation on the functionalized glass surface.

Fig. 6 below, which presents the results of the images generated by μLIBS.

By studying the effect of functionalization of the glass support, interesting results can be seen concerning the distribution of the NPs on the functionalized glass support, with respect to the increase in the analytical sensitivity of the method for detecting Au-NPs and Ag-NPs. Specifically, observing the μLIBS images of the non-functionalized glass support (Fig. 6 left), it is evident that for both Au-NPs and Ag-NPs, there is a mainly irregular distribution of NPs, characterized by the crowding of the NPs at the edges of the wells of the support. This is due to weak nanoparticle interfacial adhesion on the glass surface, where Brownian motion is the main NP surface diffusion mechanism.[65] On the other hand, comparing the LIBS images of gold and silver nanoparticles on the functionalized glass support (Fig. 6 right) presents a completely different scenario. The results show a more uniform distribution of the NPs on the wells of the functionalized glass support. This is because the chemical functionalization of the support promotes the adhesion of the NPs to the surface of the support due to the electrostatic attraction with the terminal –SH groups and the subsequent formation of the sulfur bonds. This situation causes the attachment of the NPs on the surface of the functionalized glass support, promoting their ordered and structured diffusion, as previously presented in Fig. 5. All this evidence justifies the strategic nature of the use of the μLIBS technique, not only for the quantification of NPs but also to study the distribution of metallic nanoparticles on functionalized or non-functionalized surfaces.

Given the difficulties inherent to the analysis of the NPs of interest, especially those related to the sample treatment procedures that involve the use of sophisticated separation techniques, this custom-designed functionalized glass support represents an important technological development since it allows the capture of the NPs of interest in a selective manner, completely eliminating the complicated sample treatment procedures and enabling rapid and direct analysis by the LIBS technique, as we present later. It is important to highlight that, for the functionalization of the glass support, a great diversity of functional groups can be used, which enables a very wide possibility for the development of analytical strategies for the selective and specific capture of NPs of different metals, with no size restrictions, using different functional groups on the surface of the glass support. The main advantage of using this type of functionalized glass support is that, in the case of sample analysis, it can be used in several ways: (1) by directly immersing the support in the liquid samples or (2) by depositing liquid samples in the wells of the support. This also makes it possible to study solid matrices such as soil samples and ashes of biological samples dissolved in aqueous solutions or, alternatively, gaseous samples previously dissolved in water. The metal nanoparticles present in the samples will be captured by the active functional groups on the surface of the support, so the quantification result is a direct result of the presence of the sample nanoparticles, due to their selective and specific trapping.

3.2. LIBS spectra of the functionalized glass support with Au-NPs and Ag-NPs

The spectrum obtained in the LIBS analysis of the Au-NPs is shown in Fig. 7. It is clearly observed that at a wavelength of

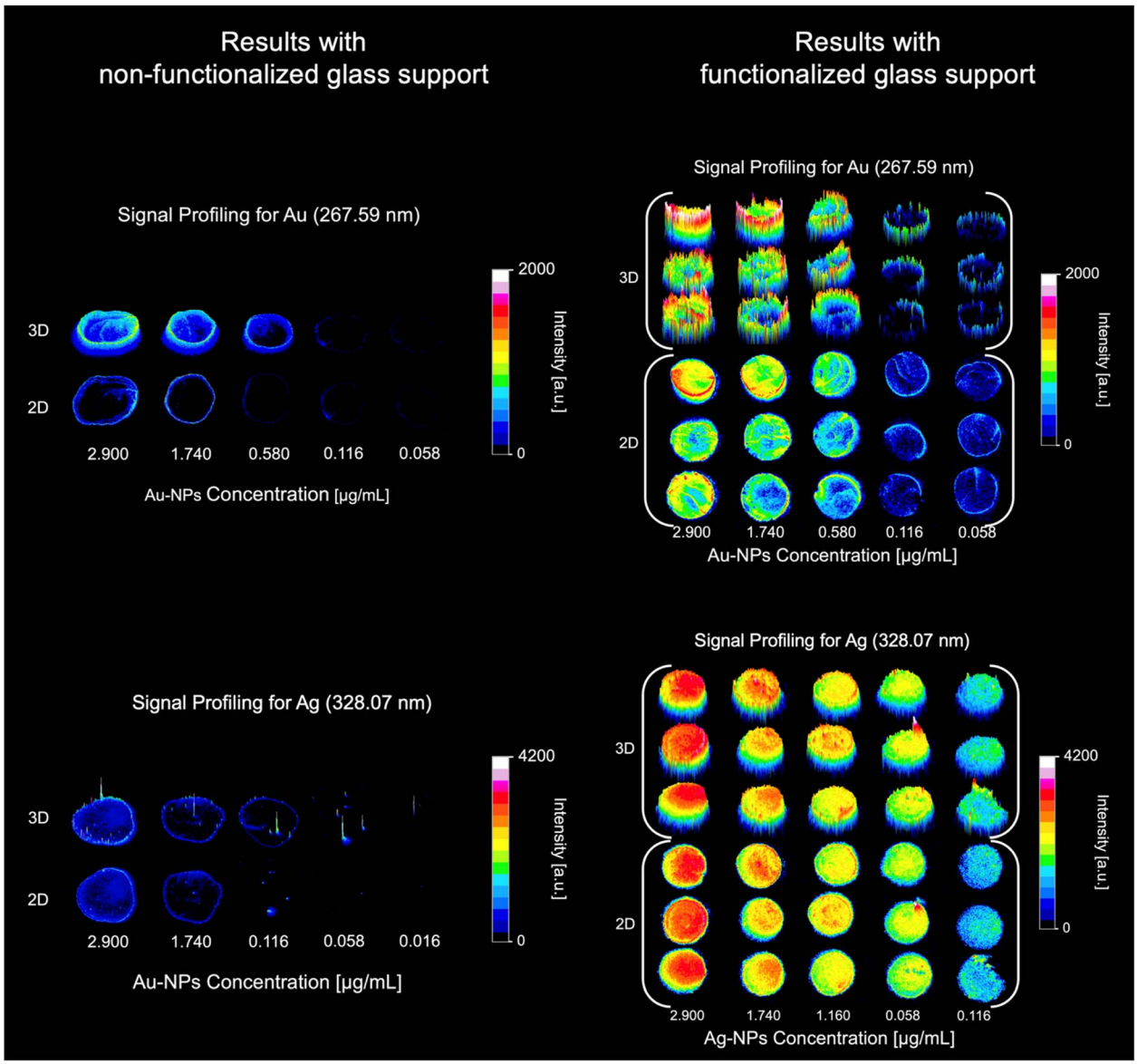

Fig. 6 Functionalized glass support µLIBS images. (Top-left) Au-NPs in a non-functionalized glass support. (Bottom-left) Ag-NPs in a non-functionalized glass support. (Top-right) Au-NPs in a functionalized glass support. (Bottom-right) Ag-NPs in a functionalized glass support.

267.59 nm, specific for one of the main emission lines of gold (Au I: $^2p^0$–^2s),[66] it is possible to detect the Au-NPs without interference from other elements that could be in the sample, either in the nanoparticle solutions or in the glass support functionalized with silane groups. Note the intense signal at 263.12 nm, which is characteristic of Si (Si I: $^1p^0$–^1s),[66] one of the main constituents of the functionalized glass support.

The LIBS spectrum obtained in the analysis of Ag-NPs is shown in Fig. 8. Note that at 328.07 nm, the characteristic signal for the Ag (Ag I: $^2p^0$–^2s)[66] emission is obtained without interference from other elements. This showed and supported the high selectivity with which the signals are detected, one of the advantages of using the LIBS technique to analyse the MNPs of the metals used in this study.

Given the presence of other chemical elements in the matrix of the colloidal solutions of nanoparticles prepared in this study, in addition to the Au and Ag line emission signals presented in the spectra in Fig. 7 and 8, the variation of other elemental lines with respect to the concentration of the substances constituting the matrix is expected to be observed. Since LIBS can detect specific and selective emission signals for each chemical element, this variation in the signals of elements other than the analyte of interest is not a major concern.

3.3. Au-NP and Ag-NP calibration curves

The calibration curves obtained for Au-NPs and Ag-NPs attached to the functionalized glass support by the LIBS technique, using the functionalized and non-functionalized glass supports, are shown in Fig. 9. Functionalizing the glass support (Fig. 9b and d) was observed to give significantly better results than those

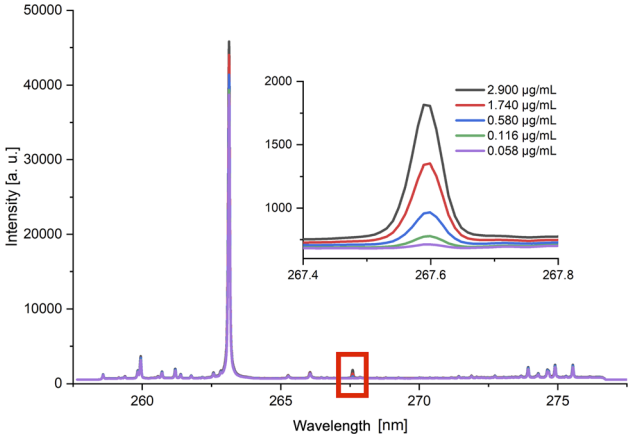

Fig. 7 Au-NP LIBS spectra of the glass support previously functionalized with silane groups. The figure shows the spectrum in the spectral range of 257.60–277.50 nm and the region of interest of 267.50 nm is broadened, specific to one of the main emission lines of gold, for each of the working solutions of five different concentration levels used.

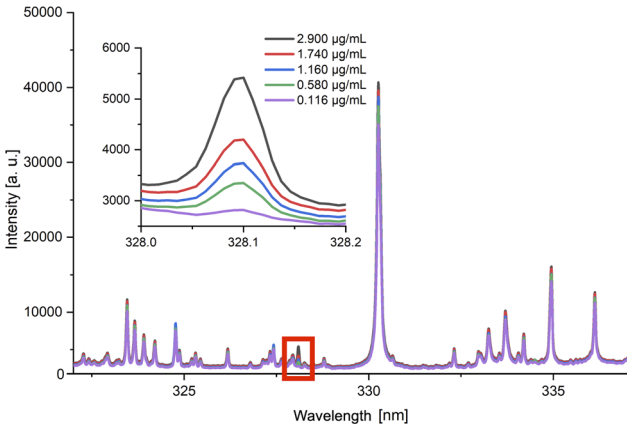

Fig. 8 Ag-NP LIBS spectra of the glass support previously functionalized with silane groups. The figure shows the spectrum in the spectral range of 327.07 nm–336.50 nm, and the region of interest of 328.07 nm is broadened, specific to one of the main emission lines of silver, for each of the working solutions of five different concentration levels used.

obtained with the non-functionalized glass support (Fig. 9a and c). When visually comparing the calibration curves, we clearly observed that the calibration curves obtained from the measurements made on the functionalized glass support show much narrower confidence bands (dark pink bands) and prediction bands (light pink bands), associated with greater precision and accuracy than the calibration curves made with the measurements obtained on the non-functionalized glass support.

By analysing the statistical results of the calibrations, compiled in Table 1, some interesting inferences can be made about the advantages of silane-functionalization on the glass support. Specifically, in the case of Au-NPs, an increase in the linearity of the calibration is observed in terms of the coefficient of determination, which increases from 0.9694 to 0.9966 when performing the detection on the functionalized glass support. In terms of sensitivity, we observe that the calibration slope obtained with the functionalized glass support increases by 4.7% compared to the slope obtained with the non-functionalized glass support, representing a slight increase in sensitivity due to functionalization.

In the case of Ag-NPs, it is observed that by using the functionalization of the glass support, the linearity of the calibration is tremendously improved. This is observed in an increase of up to 3.8 times in the coefficient of determination obtained in the calibration with the non-functionalized glass support, which increased from 0.2640 to 0.9973 on functionalization of the support. Similar results are observed with respect to sensitivity since the slope of the calibration curve with the non-functionalized glass support (106.00 [µg mL^{-1}]) increased to 455.13 (µg mL^{-1}), which constitutes an increase of 329.2% due to functionalization. Additionally, due to the functionalized glass support, a tremendously important decrease in the slope error and intercept of the calibration curves is observed. Specifically, the functionalization allows a 68% improvement, or decrease, in the error of both the slope and the calibration intercept for Au-NPs. The decrease in the slope and intercept error of the calibration of Ag-NPs was 87%. These inferences provide an analytical justification of relevance to support the increased detection capability of Au-NPs and Ag-NPs with the LIBS technique, using the functionalized glass support designed for nanoparticle capture.

As we discussed in the introduction, some relevant studies in the field of the use of LIBS for the detection of metallic nanoparticles have shown a dependence of the slope of the calibration curve on the size of the nanoparticles analyzed.[32,33,67] However, the results of this work, specifically those presented in Fig. 6, imply that the use of the functionalized glass support allows the surface consolidation of a metallic monolayer consisting of the nanoparticles so that at the time of analysis, the nanoparticles will behave as a metallic film or monolayer[59,61,68] instead of individual nanoparticles, thus obviating the limitations related to slope dependence on the particle size to be used for the calibration. Another important aspect related to this is that when using the functionalized glass support for the capture of metal nanoparticles in real samples, it is understood that the size distribution of the nanoparticles may vary significantly, *i.e.*, real samples may contain nanoparticles of various sizes, which would make it difficult to select the nanoparticle size to be used for calibration, which is a major difficulty when using LIBS for this type of analysis. However, the use of the functionalized glass support for the entrapment of nanoparticles, which favours their subsequent consolidation into a monolayer or metal film, constitutes a key strategy to facilitate LIBS analysis since instead of analysing nanoparticles suspended in an aqueous medium, analysis is performed on thin metal films for which the LIBS technique has demonstrated its analytical suitability and convenience,[69–75] without the problem of the dependence of the slope of the calibration curve on the particle size.

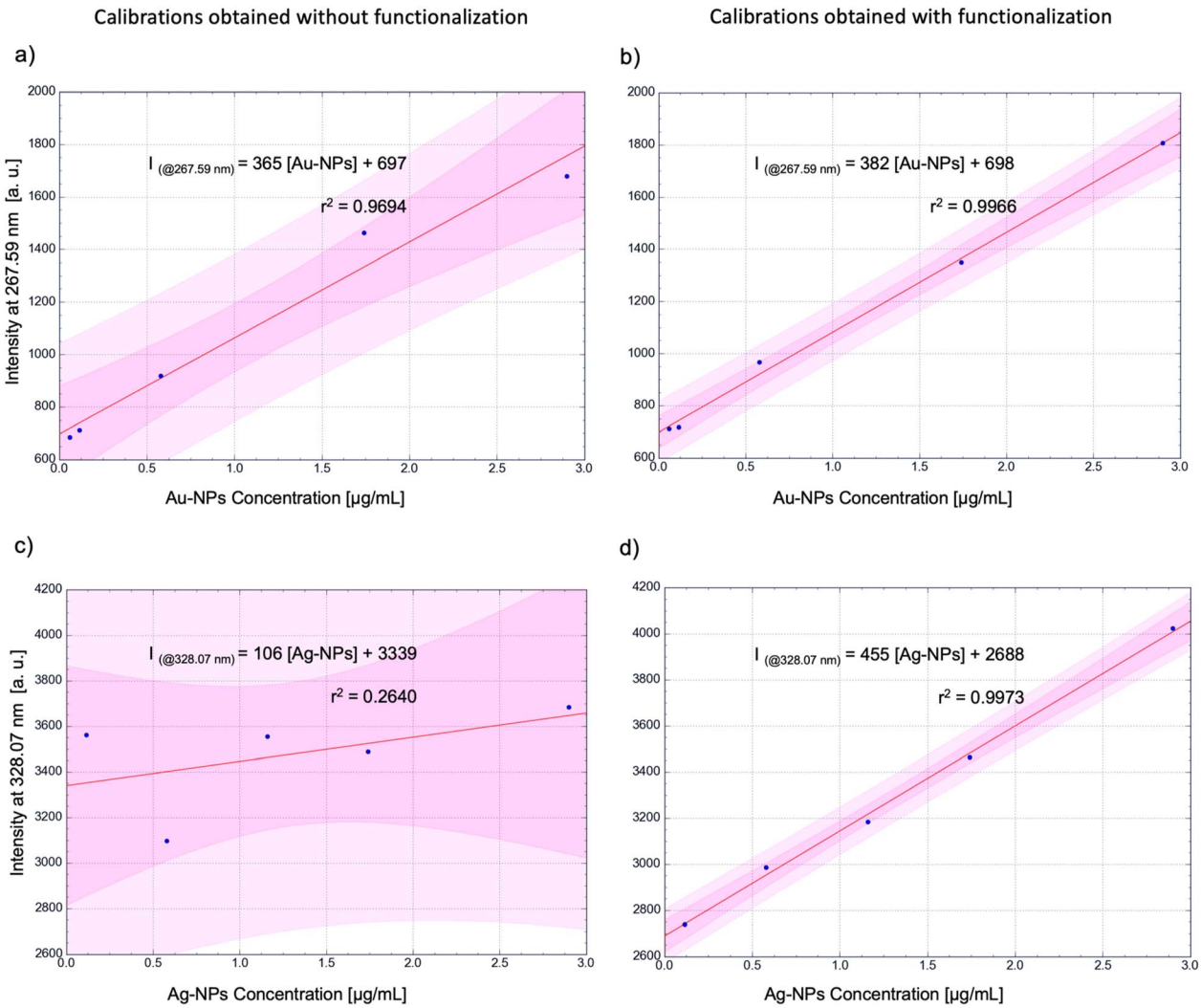

Fig. 9 Calibration curves for metallic nanoparticle quantification. (a) Scatterplot of the average intensities ($n = 3$) of working solutions at 267.59 nm as a function of the Au-NP concentration (µg mL^{-1}), adjusted with the linear model fit ($r^2 = 0.9694$), obtained with the non-functionalized glass support. (b) Scatterplot of the average intensities ($n = 3$) of working solutions at 267.59 nm as a function of the Au-NP concentration (µg mL^{-1}), adjusted with the linear model fit ($r^2 = 0.9966$), obtained with the functionalized glass support. (c) Scatterplot of the average intensities ($n = 3$) of working solutions at 328.07 nm as a function of the Ag-NP concentration (µg mL^{-1}), adjusted with the linear model fit ($r^2 = 0.9973$), obtained with the non-functionalized glass support. (d) Scatterplot of the average intensities ($n = 3$) of working solutions at 328.07 nm as a function of the Ag-NP concentration (µg mL^{-1}), adjusted with the linear model fit ($r^2 = 0.9973$), obtained with the functionalized glass support. In all graphs, the dark pink shadow shows the confidence band, and the light pink shadow shows the prediction band.

Table 1 Statistical information of the calibration curves for quantification of Au and Ag solid metallic nanoparticles

Functionalized glass support		Determination coefficient (r^2)	Slope (raw sensitivity) I (µg mL^{-1})	Intercept (intensity, a.u.)	Sensitivity increase[a] (%)
Au-NPs 19 nm	No	0.9694	365 ± 37	697 ± 57	4.7
	Yes	0.9966	382 ± 12	698 ± 19	
Ag-NPs 23 nm	No	0.2640	106 ± 102	3339 ± 165	329.2
	Yes	0.9973	455 ± 13	2688 ± 22	

[a] Calculated for a comparison of the slopes obtained with functionalized and non-functionalized glass supports.

4. Conclusions

This research shows that the LIBS technique offers high selectivity for identifying Au and Ag nanoparticles immobilized on silane-functionalized glass slides and a conveniently low linear range for quantifying the nanoparticles of interest. The proposed method, based on the LIBS technique, provides, in addition, excellent analytical results in a fast and

straightforward manner, and does not require the use of complex sample pretreatment or the use of expensive instrumentation and solvents/reagents commonly used with ICP-MS-based techniques, nor does it require complex chemometric or statistical treatments for data processing. On the other hand, the functionalized glass support designed in this research constitutes a simple and easy technological development to directly collect samples in the liquid state without the need for special pre-concentration treatments conventionally required to analyze metallic nanoparticles with other methods such as ICP-MS-based techniques. These results contribute to paving the way for the future development of LIBS-based sensors and biosensors, opening a new field of applications based on this application technique. Overall, the results reveal the potential suitability of LIBS as an emerging and analytically strategic process for the rapid, economical, and easy-to-perform analysis of metallic nanoparticles with this custom-designed functionalized glass support.

Author contributions

Jafet Cárdenas-Escudero: conceptualization, methodology, investigation, formal analysis, writing – original draft, writing – review & editing, visualization. Vincent Gardette: methodology, formal analysis, review & editing. Anabel Villalonga: methodology, investigation, formal analysis, writing – review & editing. Alfredo Sánchez: conceptualization, methodology, writing – review & editing, resources. Reynaldo Villalonga: research, formal analysis, writing – review & editing, resources, data curation, validation. Vincent Motto-Ros: conceptualization, methodology, data curation, writing – review & editing, resources, supervision. D. Galán-Madruga: methodology, formal analysis, writing – original draft. J. O. Cáceres: conceptualization, methodology, formal analysis, writing – original draft/review & editing, resources, project administration, funding acquisition, supervision.

Conflicts of interest

The authors declare that they have no known competing financial interests or personal relationships that could have appeared to influence the work reported in this paper.

Acknowledgements

The authors gratefully acknowledge the research projects PID2021-125723NB-I00 (Spanish Ministry of Economy and Competitiveness), PR27/21-015 (Complutense University and Madrid Government), and CPP2022-009754 (Spanish Ministry of Science and Innovation), for the financial support to develop this study. The authors also thank to the Université Lyon 1 – CNRS Institut Lumière Matière. J. Cárdenas-Escudero specially thanks to Universidad de Panamá and Instituto para la Formación y Aprovechamiento de los Recursos Humanos de Panamá (IFARHU) for the financial support for his doctoral studies.

References

1 S. Kumar, B. Kumar, R. Sehgal, M. F. Wani, D. Kumar, M. D. Sharma, V. Singh, R. Sehgal and V. Kumar, in *Nanoparticles Reinforced Metal Nanocomposites: Mechanical Performance and Durability*, ed. S. K. Tiwari, V. Kumar and S. Thomas, Springer Nature Singapore, Singapore, 2023, pp. 209–235, DOI: 10.1007/978-981-19-9729-7_7.
2 D. T. Thompson, *Nano Today*, 2007, **2**, 40–43.
3 A. Sápi, T. Rajkumar, J. Kiss, Á. Kukovecz, Z. Kónya and G. A. Somorjai, *Catal. Lett.*, 2021, **151**, 2153–2175.
4 H.-L. Tan, S.-Y. Teow and J. Pushpamalar, *Bioengineering*, 2019, **6**, 17.
5 M. Rai, A. P. Ingle, S. Birla, A. Yadav and C. A. D. Santos, *Crit. Rev. Microbiol.*, 2016, **42**, 696–719.
6 Y. Li, Q. Liang, L. Zhou, J. Liu and Y. Liu, *J. Nanopart. Res.*, 2022, **24**, 84.
7 E. Tinajero-Díaz, D. Salado-Leza, C. Gonzalez, M. Martínez Velázquez, Z. López, J. Bravo-Madrigal, P. Knauth, F. Y. Flores-Hernández, S. E. Herrera-Rodríguez, R. E. Navarro, A. Cabrera-Wrooman, E. Krötzsch, Z. Y. G. Carvajal and R. Hernández-Gutiérrez, *Pharmaceutics*, 2021, **13**, 1719.
8 C. Moşoarcă, R. Bănică and P. Linul, in *New Frontiers in Nanochemistry*, Apple Academic Press, 2020, pp. 327–337.
9 T. Patil, R. Gambhir, A. Vibhute and A. P. Tiwari, *J. Cluster Sci.*, 2023, **34**, 705–725.
10 P. G. Jamkhande, N. W. Ghule, A. H. Bamer and M. G. Kalaskar, *J. Drug Delivery Sci. Technol.*, 2019, **53**, 101174.
11 E. Cavaliere, S. De Cesari, G. Landini, E. Riccobono, L. Pallecchi, G. M. Rossolini and L. Gavioli, *Nanomed. Nanotechnol. Biol. Med.*, 2015, **11**, 1417–1423.
12 P. Rani, R. S. Varma, K. Singh, R. Acevedo and J. Singh, *Chemosphere*, 2023, **317**, 137841.
13 M. N. A. Azeem, O. M. Ahmed, M. Shaban and K. N. M. Elsayed, *Environ. Sci. Pollut. Res.*, 2022, **29**, 59930–59947.
14 P. Das, K. Ghosal, N. K. Jana, A. Mukherjee and P. Basak, *Mater. Chem. Phys.*, 2019, **228**, 310–317.
15 M. Ali, *Adv. Colloid Interface Sci.*, 2023, **314**, 102881.
16 C. A. Dos Santos, M. M. Seckler, A. P. Ingle, I. Gupta, S. Galdiero, M. Galdiero, A. Gade and M. Rai, *J. Pharm. Sci.*, 2014, **103**, 1931–1944.
17 I. Fratoddi, I. Venditti, C. Cametti and M. V. Russo, *Nano Res.*, 2015, **8**, 1771–1799.
18 W. Hu, C. Wang, D. Gao and Q. Liang, *J. Appl. Toxicol.*, 2023, **43**, 32–46.
19 J. K. Suthar, A. Vaidya and S. Ravindran, *J. Appl. Toxicol.*, 2023, **43**, 4–21.
20 M. Noga, J. Milan, A. Frydrych and K. Jurowski, *Int. J. Mol. Sci.*, 2023, **24**, 5133.
21 G. R. Tortella, O. Rubilar, N. Durán, M. C. Diez, M. Martínez, J. Parada and A. B. Seabra, *J. Hazard. Mater.*, 2020, **390**, 121974.

22 T. Jaswal and J. Gupta, *Mater. Today: Proc.*, 2021, **81**, 859–863.
23 C. Levard, E. M. Hotze, G. V. Lowry and G. E. Brown Jr, *Environ. Sci. Technol.*, 2012, **46**, 6900–6914.
24 S. M. Majedi and H. K. Lee, *TrAC, Trends Anal. Chem.*, 2016, **75**, 183–196.
25 I. Hagarová, *Anal. Methods*, 2017, **9**, 3594–3601.
26 Q. Bai, Y. Yin, Y. Liu, H. Jiang, M. Wu, W. Wang, Z. Tan, J. Liu, M. H. Moon and B. Xing, *Appl. Spectrosc. Rev.*, 2023, **58**, 110–131.
27 K. Keerthi, S. D. George, S. D. Kulkarni, S. Chidangil and V. K. Unnikrishnan, *Opt Laser. Technol.*, 2022, **147**, 107622.
28 R. Noll, C. Fricke-Begemann, S. Connemann, C. Meinhardt and V. Sturm, *J. Anal. At. Spectrom.*, 2018, **33**, 945–956.
29 S. Legnaioli, G. Lorenzetti, L. Pardini, G. H. Cavalcanti and V. Palleschi, in *Laser-Induced Breakdown Spectroscopy: Theory and Applications*, ed. S. Musazzi and U. Perini, Springer Berlin Heidelberg, Berlin, Heidelberg, 2014, pp. 169–193, DOI: **10.1007/978-3-642-45085-3_7**.
30 F. Zhang, Q. Wang, Y. Jiang, A. Chen and M. Jin, *Spectrochim. Acta, Part B*, 2023, **201**, 106626.
31 Z. H. Khan, M. H. Ullah, B. Rahman, A. I. Talukder, M. Wahadoszamen, K. M. Abedin and A. F. M. Y. Haider, *J. Spectrosc.*, 2022, **2022**, 3887038.
32 A. De Giacomo, R. Gaudiuso, C. Koral, M. Dell'Aglio and O. De Pascale, *Spectrochim. Acta, Part B*, 2014, **98**, 19–27.
33 A. De Giacomo, R. Gaudiuso, C. Koral, M. Dell'Aglio and O. De Pascale, *Anal. Chem.*, 2013, **85**, 10180–10187.
34 B. Mayol, P. Díez, A. Sánchez, C. de la Torre, A. Villalonga, E. Lucena-Sánchez, F. Sancenón, P. Martínez-Ruiz, D. Vilela, R. Martínez-Máñez and R. Villalonga, *Nanoscale*, 2021, **13**, 18616–18625.
35 P. Mendis, R. M. de Silva, K. M. N. de Silva, L. A. Wijenayaka, K. Jayawardana and M. Yan, *RSC Adv.*, 2016, **6**, 48792–48799.
36 X. Liu, M. Atwater, J. Wang and Q. Huo, *Colloids Surf., B*, 2007, **58**, 3–7.
37 D. Paramelle, A. Sadovoy, S. Gorelik, P. Free, J. Hobley and D. G. Fernig, *Analyst*, 2014, **139**, 4855–4861.
38 M. E. Marques, A. A. P. Mansur and H. S. Mansur, *Appl. Surf. Sci.*, 2013, **275**, 347–360.
39 A. Kramida, K. Olsen and Y. Ralchenko, National Institute of Standards and Technology web, **https://physics.nist.gov/PhysRefData/ASD/LIBS/libs-form.html**, 2023.
40 Y. Q. He, S. P. Liu, L. Kong and Z. F. Liu, *Spectrochim. Acta, Part A*, 2005, **61**, 2861–2866.
41 M. Hlaing, B. Gebear-Eigzabher, A. Roa, A. Marcano, D. Radu and C.-Y. Lai, *Opt. Mater.*, 2016, **58**, 439–444.
42 J. Turkevich, P. C. Stevenson and J. Hillier, *Discuss. Faraday Soc.*, 1951, **11**, 55–75.
43 G. Frens, *Nat. Phys. Sci.*, 1973, **241**, 20–22.
44 J. Kimling, M. Maier, B. Okenve, V. Kotaidis, H. Ballot and A. Plech, *J. Phys. Chem. B*, 2006, **110**, 15700–15707.
45 P. Zhao, N. Li and D. Astruc, *Coord. Chem. Rev.*, 2013, **257**, 638–665.
46 J. Dong, P. L. Carpinone, G. Pyrgiotakis, P. Demokritou and B. M. Moudgil, *Kona*, 2020, **37**, 224–232.
47 Ratyakshi and R. Chauhan, *Asian J. Chem.*, 2009, **21**, 113–116.
48 F. Beck, M. Loessl and A. J. Baeumner, *Microchim. Acta*, 2023, **190**, 91.
49 Z. Xiao, H. Meng, X. Qin, X. Sang, Y. Zhang and Y. Yuan, *Analyst*, 2021, **146**, 597–604.
50 S. Zhan, C. Xu, J. Chen, Q. Xiao, Z. Zhou, Z. Xing, C. Gu, Z. Yin and H. Liu, *Electrochim. Acta*, 2023, **437**, 141468.
51 H.-M. Kim, H.-J. Kim, J.-H. Park and S.-K. Lee, *Anal. Chim. Acta*, 2022, **1213**, 339960.
52 N. Thomas, P. Sreekeerthi and P. Swaminathan, *Phys. Chem. Chem. Phys.*, 2022, **24**, 25025–25035.
53 W. Shen, L. Zhang, X. Li and H.-Z. Yu, *Sci. Rep.*, 2019, **9**, 9172.
54 L. Wang, U. S. Schubert and S. Hoeppener, *Chem. Soc. Rev.*, 2021, **50**, 6507–6540.
55 K. Wieszczycka, K. Staszak, M. J. Woźniak-Budych, J. Litowczenko, B. M. Maciejewska and S. Jurga, *Coord. Chem. Rev.*, 2021, **436**, 213846.
56 N. Linares, E. Serrano, M. Rico, A. Mariana Balu, E. Losada, R. Luque and J. García-Martínez, *Chem. Commun.*, 2011, **47**, 9024–9035.
57 F. Pena-Pereira, R. M. B. O. Duarte and A. C. Duarte, *TrAC, Trends Anal. Chem.*, 2012, **40**, 90–105.
58 D. L. Kokkin, R. Zhang, T. C. Steimle, I. A. Wyse, B. W. Pearlman and T. D. Varberg, *J. Phys. Chem. A*, 2015, **119**, 11659–11667.
59 H. Häkkinen, *Nat. Chem.*, 2012, **4**, 443–455.
60 H. Kitching, A. J. Kenyon and I. P. Parkin, *Phys. Chem. Chem. Phys.*, 2014, **16**, 6050–6059.
61 H. S. Toh, C. Batchelor-McAuley, K. Tschulik and R. G. Compton, *Sci. China: Chem.*, 2014, **57**, 1199–1210.
62 E. Csapó, R. Patakfalvi, V. Hornok, L. T. Tóth, Á. Sipos, A. Szalai, M. Csete and I. Dékány, *Colloids Surf., B*, 2012, **98**, 43–49.
63 W.-H. Chen, Y.-T. Tseng, S. Hsieh, W.-C. Liu, C.-W. Hsieh, C.-W. Wu, C.-H. Huang, H.-Y. Lin, C.-W. Chen, P.-Y. Lin and L.-K. Chau, *RSC Adv.*, 2014, **4**, 46527–46535.
64 T.-J. Lee, L.-K. Chau and C.-J. Huang, *Langmuir*, 2020, **36**, 5935–5943.
65 M. José-Yacamán, C. Gutierrez-Wing, M. Miki, D. Q. Yang, K. N. Piyakis and E. Sacher, *J. Phys. Chem. B*, 2005, **109**, 9703–9711.
66 A. Kramida, Y. Ralchenko, J. Reader and NIST ASD Team, *NIST Atomic Spectra Database (version 5.11)*, National Institute of Standards and Technology, Gaithersburg, MD, 2023, DOI: **10.18434/T4W30F**.
67 J. E. Carranza and D. W. Hahn, *Anal. Chem.*, 2002, **74**, 5450–5454.
68 P. Pallavicini, A. Taglietti, G. Dacarro, Y. Antonio Diaz-Fernandez, M. Galli, P. Grisoli, M. Patrini, G. Santucci De Magistris and R. Zanoni, *J. Colloid Interface Sci.*, 2010, **350**, 110–116.
69 S. Messaoud Aberkane, M. Abdelhamid, K. Yahiaoui, C. Mahieddoune, S. Abdelli-Messaci and M. A. Harith, *Thin Solid Films*, 2018, **653**, 293–300.
70 M. Abdelhamid, S. Grassini, E. Angelini, G. M. Ingo and M. A. Harith, *Spectrochim. Acta, Part B*, 2010, **65**, 695–701.

71 S. Liu, Q. Gao, J. Xiu, Z. Li and Y. Liu, *Spectrochim. Acta, Part B*, 2019, **160**, 105684.
72 E. Axente, J. Hermann, G. Socol, L. Mercadier, S. A. Beldjilali, M. Cirisan, C. R. Luculescu, C. Ristoscu, I. N. Mihailescu and V. Craciun, *J. Anal. At. Spectrom.*, 2014, **29**, 553–564.
73 A. Jurado-López and M. D. Luque de Castro, *J. Anal. At. Spectrom.*, 2002, **17**, 544–547.
74 J. Xiu, S. Liu, S. Fu, T. Wang, M. Meng and Y. Liu, *Appl. Opt.*, 2019, **58**, 1040–1047.
75 J. Xiu, S. Liu, M. Sun and L. Dong, *Appl. Opt.*, 2018, **57**, 404–408.